

Photometric Stereo with Near Point Lighting: A Solution by Mesh Deformation

Wuyuan Xie, Chengkai Dai, and Charlie C. L. Wang*

Department of Mechanical and Automation Engineering, The Chinese University of Hong Kong
Shatin, N.T., Hong Kong

cwang@mae.cuhk.edu.hk

Abstract

We tackle the problem of photometric stereo under near point lighting in this paper. Different from the conventional formulation of photometric stereo that assumes parallel lighting, photometric stereo under the near point lighting condition is a nonlinear problem as the local surface normals are coupled with its distance to the camera as well as the light sources. To solve this non-linear problem of PS with near point lighting, a local/global mesh deformation approach is developed in our work to determine the position and the orientation of a facet simultaneously, where each facet is corresponding to a pixel in the image captured by the camera. Unlike nonlinear optimization schemes, the mesh deformation in our approach is decoupled into an iteration of interlaced steps of local projection and global blending. Experimental results verify that our method can generate accurate estimation of surface shape under near point lighting in a few iterations. Besides, this approach is robust to errors on the positions of light sources and is easy to be implemented.

1. Introduction

Photometric stereo (PS) [1] estimates a dense field of normals from a set of 2D images captured by a fix camera under different illumination conditions. In the framework of PS, it is assumed that objects to be reconstructed all have a Lambertian surface and are illuminated by at least three known lighting directions. As a result, the normal vector at each pixel can be determined from the captured image intensities uniquely (or by a least-square solution when more than three images are taken). Such a simple principle makes PS as an old but distinctive topic in computer vision developed for decades. Different from other approaches based on the triangulation theorem, PS has advantage on capturing the geometry details in high frequency but has defects in reconstructing good overall shapes in low frequency. Therefore, PS technique has been employed to reconstruct geometric textures together with other triangulation-based

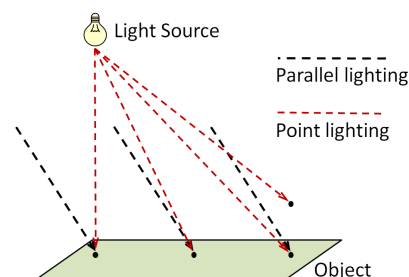


Figure 1. An illustration for the near point lighting (NPL) model: different from the parallel lighting, the lighting direction in NPL varies with the change of positions.

methods (e.g., [2]). The shape distortions generated by PS in low frequency is mainly caused by the following three assumptions in the framework of conventional PS computation:

- First, to make the problem simple, camera sensor is assumed to use orthogonal projection in the framework of PS.
- Second, to avoid considering shadow and specularity in the radiance equation, all interested points are assumed to obey Lambertian reflection ideally.
- Last but not least, light sources are assumed to be located at infinite positions so that the illumination can be regarded as parallel lighting.

Based on these three assumptions, the lighting model of PS problem can be linearized into a set of linear equations to be solved by the least-square solution. A lot of effort has been conducted in prior research to make the real condition under illumination to approach these assumptions. For example, the projection of camera sensor can be assumed as orthogonal when distance between the camera and the object under acquisition is small. Approaches have been investigated to recover the regions with shadow and/or specularity (e.g., [3,4]). To achieve parallel lighting condition, existing approaches usually place light sources far away from the object. However, this will make the luminance attenuate

sharply to result in images with poor quality. In this paper, we provide a solution to the problem of *near point lighting PS* (NPL-PS) to overcome this limitation.

Without loss of generality, the input of our NPL-PS approach has k images, $\mathcal{I}_1, \dots, \mathcal{I}_k$, where each has the same interested region composing of m pixels. The image \mathcal{I}_i is captured under the illumination of the i -th lighting source with its position $\mathbf{p}_i \in \mathbb{R}^3$ known. As illustrated in Fig.1, different surface points have different lighting directions under the illumination of near point lighting. The lighting direction at a point corresponding to a pixel in the image space not only varies with the change of image coordinates but also changes according to the depth. In short, the radiation model correlating the captured light intensities and the height/orientation of a surface region is nonlinear.

Main Result: In this paper, we propose a simple but novel approach to solve the NPL-PS problem that can generate a 3D mesh surface from a set of 2D images, $\{\mathcal{I}_i\}$, under the exposure of different near point lighting sources. Each pixel in the interested region in input images is represented as a polygonal facet to form a piecewise linear surface \mathcal{M} . We assume the surface region to be reconstructed here is C^0 -continuous. The nonlinear NPL-PS problem is solved by a mesh deformation approach with iteratively applied local shaping and global blending steps (see Fig.2 for an example). Our method avoids to apply either the conventional integration (e.g., [5]) or the time-consuming nonlinear optimization (e.g., [6]). Only simple linear operations are taken during the iterations of our approach. As a result, a 3D mesh surface can be efficiently and robustly obtained after a few steps of mesh deformation. Both the geometric details in high frequency and the overall shapes in low frequency can be accurately reconstructed on the resultant mesh surface.

The rest of the paper is organized as follows. Section 2 reviews the related work of photometric stereo and mesh deformation based shape optimization. We analyze and compare the difference between conventional PS and *near point lighting PS* (NPL-PS) in Section 3. After that, the formulation for solving the NPL-PS problem is detailed in Section 4. Lastly, experimental results are given in Section 5, and our paper ends with the conclusion section.

2. Related Work

Prior works have paid a lot of attention to improve the results of PS-based reconstruction – mainly by correcting the aforementioned assumptions for linearization. The existing approaches can be roughly classified into three categories. The first category mainly focuses on improve the radiance model, where the Lambertian model is replaced by more real but complex ones (ref. [7–10]). These approaches mainly serve for surface rendering and are not good at reconstructing accurate 3D surfaces. The second category of

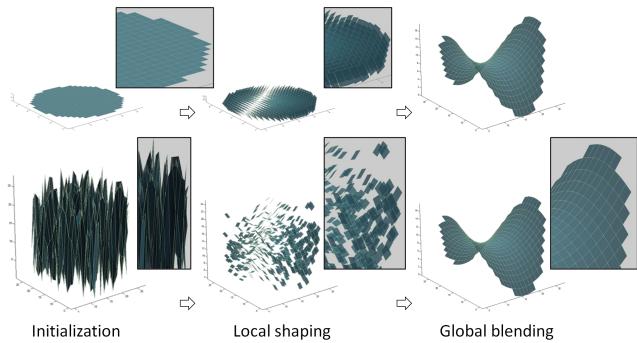


Figure 2. One step of our mesh deformation based NPL-PS: (left) an initial mesh surface before deformation, (middle) the facets are positioned along the orientation of target normals in the local shaping step, and (right) the facets are glued together into a mesh surface in the global blending step. The final result can be obtained by applying the steps of local shaping and global blending iteratively. It is easy to find that our method is trivially affected by the initial guess. When a planar initial shape (top row) or a random initial shape (bottom row) is given, the computation converges to the similar shape in just a few steps.

approaches [6, 11, 12] emphasize on how to deal with the error induced by ill reflectance points (i.e., shadows and specularities). In a typical work [6], the authors propose to use a matrix analysis approach to solve the ill PS problem with shadows and specularities. Their methods can improve the high frequency information in geometric details but are still suffered from the distortion in overall shape (i.e., errors in low frequency that are caused by the assumption of placing point lighting sources in infinity). The third group of methods (e.g., [13–17]) aim at improving the resultant shapes of PS by correcting the lighting model into NPL sources. When there is no shadow and specularity included in input images, the estimated surface normals are mainly affected by the lighting directions. If bias have been incorporated into the estimated normals, they will be further transferred to the reconstructed 3D shapes from normals. To reconstruct an accurate shape in all bands of frequencies, it is necessary to consider a more realistic lighting model. However, when a realistic non-parallel lighting model is employed, PS problem becomes nonlinear and the numerical computation based on nonlinear optimization requires other auxiliaries (e.g., some known 3D positions). In [13], a sparse depth-map or scattered 3D feature points are used for this purpose. Our approach presented in this paper overcome this difficulty by using a local/global mesh deformation technique to solve the nonlinear model.

In the literature of geometric modeling, the local/global optimization strategy has been widely used to decouple the problem of solving nonlinear optimization into interlaced orthogonal linear operations (e.g., [18, 19]). Recently, the discrete geometric processing technique has been extended to solve the surface-from-gradients problem [20]. Inspired

by this work, we develop a new method to solve the NLP-PS problem by mesh deformation. Unlike the conventional pipeline of PS that computes a dense normal field first and then conducts the surface-from-gradients technique to obtain the surface shape, we provide a one-stop solution to directly generate a 3D surface from the input 2D images. Details can be found in Section 4.

3. Linear vs. Nonlinear Photometric Stereo

In this section, we analyze the problem of conventional PS framework (i.e., linear PS) and then introduce the NLP-PS model that is nonlinear.

3.1. Conventional photometric stereo

The observed appearance brightness I of a Lambertian object under a lighting direction $\mathbf{l} \in \mathbb{R}^3$ at a surface point $\mathbf{x} \in \mathbb{R}^3$ can be described as $I(\mathbf{x}) = \rho \mathbf{n} \cdot \mathbf{l}$, where ρ is the Lambertian reflection albedo and $\mathbf{n} \in \mathbb{R}^3$ is the surface normal at \mathbf{x} . Note that, under the assumption of parallel lighting in conventional PS, the lighting direction does not change in the whole domain (i.e., \mathbf{l} is *not* a function of \mathbf{x}). There are k images, $\{\mathcal{I}_i\}$, of the same object under the illumination of different light sources, and the above lighting model is used to determine the value of \mathbf{n} at each pixel in the interested region. Specifically, when $k > 3$, the value of $\rho \mathbf{n}$ can be determined by a least-square solution of

$$I_i(\mathbf{x}) = \rho \mathbf{n} \cdot \mathbf{l}_i \quad (i = 1, \dots, k). \quad (1)$$

Here, I_i is the brightness observed in the i -th image and \mathbf{l}_i denotes the lighting direction of the i -th source. Different values of the Lambertian reflection albedo appear at different surface points. However, the value of ρ does not change at the same surface point under the illumination of different lighting directions. As a result, one can solve Eq.(1) to obtain the value of $\rho \mathbf{n}$ first, and then normalize it to obtain a unit surface normal vector \mathbf{n} . After that, the surface-from-gradients technique (e.g., [20–23]) is employed to reconstruct a 3D surface from the field of normal vectors.

3.2. Near point lighting illumination

The conventional PS assumes an object to be reconstructed is under the illumination of nearly parallel lighting. In practice, illumination is nearly parallel only when the distance between a lighting source and the object is more than 10 times of the object’s dimension [5]. However, when a light source is placed in a distance that far away from the object, the luminance will attenuate sharply and hence deteriorate the captured image. Based on this reason, light sources are usually placed close to the object to ensure the quality of images. In such circumstances, parallel lighting assumption leads to the significant shape distortion in coarse scale although the geometric details in high-frequency band can still be successfully reconstructed.

To overcome this contradiction between assumption and practice, we adopt the near point lighting (NPL) model to estimate the surface shape in this paper. Under the illumination of NPL, two important factors must be noticed.

- Every surface point has its own unique lighting direction, and all lighting directions at different regions converge at the same point light source.
- The attenuation of luminance needs to be considered in the Lambertian radiance model (i.e., distances between surface points and light sources should be incorporated into the model).

Therefore, akin to the lighting model presented in [12], we employ a NPL model as

$$I_i(\mathbf{x}) = \frac{\rho}{\alpha \|\mathbf{p}_i - \mathbf{x}\|^2} \left(\mathbf{n}(\mathbf{x}) \cdot \frac{\mathbf{p}_i - \mathbf{x}}{\|\mathbf{p}_i - \mathbf{x}\|} \right), \quad (2)$$

where α is the attenuation coefficient, \mathbf{p}_i is the position of the i -th light source, and therefore $(\mathbf{p}_i - \mathbf{x})/\|\mathbf{p}_i - \mathbf{x}\|$ gives the lighting direction \mathbf{l}_i at \mathbf{x} . The difference between this illumination model and the conventional illumination model in PS has been illustrated in Fig.1.

In our NPL model, the position of light sources can be obtained by a calibration procedure [24] when the relative position between camera and light sources are fixed during the shape acquisition. Even after determining the positions of light sources, Eq.(2) is still non-linear due to the unknown depth value of \mathbf{x} for each pixel in the captured images. In the following, we investigate a method to solve the values of $\mathbf{n}(\mathbf{x})$ and \mathbf{x} simultaneously based on local/global mesh deformation. Besides the positions of light sources, our method also needs to know the corresponding width w and height h of a pixel in the captured images – i.e., scale of the image coordinates to the Euclidean coordinates, which can also be obtained from the calibration procedure.

4. Formulation in Mesh Deformation

Our formulation for solving the NPL-PS problem is based on converting each pixel (i, j) in the interested region into a quadrangular facet $f_{i,j}$, the boundary of which is defined by four vertices $\mathbf{v}_{i,j}$, $\mathbf{v}_{i+1,j}$, $\mathbf{v}_{i+1,j+1}$ and $\mathbf{v}_{i,j+1}$. A vertex $\mathbf{v}_{i,j}$ has its x - and y -coordinates fixed and $z_{i,j}$ as an unknown variable to be determined – that is $(o_x + iw, o_y + jh, o_z + z_{i,j})$. Here (o_x, o_y, o_z) specifies the shifting between the image coordinate system and the world coordinate system. The initial values of $z_{i,j}$ can be assigned as $z_{i,j} = 0$ or be given randomly. The following formulation will provide an efficient method to determine their values to satisfy Eq.(2) on all facets/pixels. The collection of facets forms a mesh surface \mathcal{M} with C^0 -continuity.

4.1. Local/Global mesh deformation

Generally speaking, the strategy of local/global mesh deformation decouples the nonlinear optimization procedure into interlaced steps of local shaping and global blending. A mesh surface \mathcal{M} is deformed iteratively to minimize an energy function defined according to the governing conditions (e.g., enforcing normals to follow the input gradient-field).

In each iteration, a local shaping step is first performed to determine the position and orientation of each facet according to its target normal and its current shape. The mesh surface has been broken after the local shaping – see Fig.2 for an illustration. After that, a global blending step is applied to glue all the facets back into a connected mesh surface. Specifically, the global blending step minimizes a functional to reduce the difference between $\mathbf{z}(f_{i,j})$ and $\mathbf{p}(f_{i,j})$ on each facet $f_{i,j}$, where $\mathbf{z}(f_{i,j})$ is a column vector formed by the depths of $f_{i,j}$'s four vertices

$$\mathbf{z}(f_{i,j}) = \{z_{i,j}, z_{i+1,j}, z_{i+1,j+1}, z_{i,j+1}\},$$

and $\mathbf{p}(f_{i,j})$ is its corresponding vector after applying the local shaping step. Details for determining $\mathbf{p}(f_{i,j})$ can be found in Section 4.2. However, enforcing $\mathbf{z}(f_{i,j}) = \mathbf{p}(f_{i,j})$ is too restrictive, which could slow down the convergence during the iteration. To solve this problem, the functional is relaxed by applying the mean-subtraction technique (ref. [19]) as

$$\Phi(\{z_{i,j}\}) = \sum_{f_{i,j}} \|\mathbf{Nz}(f_{i,j}) - \mathbf{Np}(f_{i,j})\|^2, \quad (3)$$

where $\mathbf{N} = \mathbf{I}_{4 \times 4} - \frac{1}{4}\mathbf{1}_{4 \times 4}$ with $\mathbf{1}$ being a matrix with all elements equal to 1. It is found that Eq.(3) can be reformulated into a more compact form as

$$\Phi(\{z_{i,j}\}) = \|\mathbf{A}\mathbf{d} - \mathbf{b}\|^2, \quad (4)$$

where \mathbf{A} is a $4m \times n$ matrix derived from $\mathbf{Nz}(f_{i,j})$ and \mathbf{b} is a vector with $4m$ components derived from $\mathbf{Np}(f_{i,j})$ on a mesh surface \mathcal{M} with m quadrangular facets and n vertices. All the unknown depth values of the vertices (n in total) are listed in \mathbf{d} . This is a standard least-square problem, which can be solved by $\mathbf{A}^T\mathbf{A}\mathbf{d} = \mathbf{A}^T\mathbf{b}$. Moreover, $\mathbf{A}^T\mathbf{A}$ does not change during the iterations as the matrix \mathbf{A} only depends on the connectivity of \mathcal{M} that is invariant. As a result, we can pre-factorize $\mathbf{A}^T\mathbf{A}$ at the beginning of iterations and re-use the result of factorization in all the rest steps – the computation only involving back substitution is very efficient.

4.2. Local projection for NPL-PS

To use the local/global mesh deformation technique, we first formulate the local shaping step of each facet according to the lighting model that has been derived in Section

3 for NLP-PS. Considering about a pixel (i, j) and its corresponding facet $f_{i,j}$, two operations are taken on $f_{i,j}$ for solving the NPL-PS problem in the local shaping step: 1) determining the normal, $\mathbf{n}_{i,j}$, of $f_{i,j}$ and 2) rotating the facet to following the orientation of $\mathbf{n}_{i,j}$.

The normal $\mathbf{n}_{i,j}$ is determined at the center of $f_{i,j}$, that is $\mathbf{c}_{i,j} = \frac{1}{4}(\mathbf{v}_{i,j} + \mathbf{v}_{i+1,j} + \mathbf{v}_{i+1,j+1} + \mathbf{v}_{i,j+1})$. Thus, for the k -th image, an equation can be obtained from the nonlinear lighting model at $\mathbf{c}_{i,j}$ as

$$(\mathbf{p}_k - \mathbf{c}_{i,j}) \cdot \frac{\rho}{\alpha} \mathbf{n}_{i,j} = I_k(i, j) \|\mathbf{p}_k - \mathbf{c}_{i,j}\|^3 \quad (5)$$

$I_k(i, j)$ denotes the light intensity at the pixel (i, j) in the image \mathcal{I}_k . Incorporating all images, the normal vector $\mathbf{n}_{i,j}$ can be obtained by a least-square solution as

$$\mathbf{T} \left(\frac{\rho}{\alpha} \mathbf{n}_{i,j} \right) = \sum_k \|\mathbf{p}_k - \mathbf{c}_{i,j}\|^3 I_k(i, j) (\mathbf{p}_k - \mathbf{c}_{i,j}) \quad (6)$$

with

$$\mathbf{T} = \begin{bmatrix} \sum_k (\mathbf{a}_k^x)^2 & \sum_k (\mathbf{a}_k^x \mathbf{a}_k^y) & \sum_k (\mathbf{a}_k^x \mathbf{a}_k^z) \\ \sum_k (\mathbf{a}_k^x \mathbf{a}_k^y) & \sum_k (\mathbf{a}_k^y)^2 & \sum_k (\mathbf{a}_k^y \mathbf{a}_k^z) \\ \sum_k (\mathbf{a}_k^x \mathbf{a}_k^z) & \sum_k (\mathbf{a}_k^y \mathbf{a}_k^z) & \sum_k (\mathbf{a}_k^z)^2 \end{bmatrix} \quad (7)$$

by defining $\mathbf{a}_k = \mathbf{p}_k - \mathbf{c}_{i,j}$. The superscript in $\{x, y, z\}$ indicates the x -, y - and z -components of a vector respectively. The value of $\frac{\rho}{\alpha} \mathbf{n}_{i,j}$ can be robustly determined from Eq.(6) via *singular value decomposition* (SVD). Then, the unit vector $\mathbf{n}_{i,j}$ is computed by normalization.

After knowing $\mathbf{n}_{i,j}$, we shift the position of $f_{i,j}$'s vertices along the z -axis to put them on the plane $\mathcal{P}_{i,j}$ that passes through $\mathbf{c}_{i,j}$ and has the normal $\mathbf{n}_{i,j}$. A vector formed by depth components of the four projected vertices is defined as

$$\mathbf{p}(f_{i,j}) = \{p_{i,j}, p_{i+1,j}, p_{i+1,j+1}, p_{i,j+1}\}.$$

Here, the depth values are

$$p_{k,l} = \mathbf{c}_{i,j}^z - \frac{(k-i-\frac{1}{2})w\mathbf{n}_{i,j}^x + (l-j-\frac{1}{2})h\mathbf{n}_{i,j}^y}{\mathbf{n}_{i,j}^z} \quad (8)$$

with $k \in \{i, i+1\}$ and $l \in \{j, j+1\}$. Note that the NLP model presented in Eq.(2) is nonlinear to the center of a facet, $f_{i,j}$. In our local shaping step, we simplify the computation by using the current center of $f_{i,j}$ and leave the position of $\mathbf{c}_{i,j}$ to be updated in the global blending step of our framework.

4.3. Iteration framework for NPL-PS

The possibility allowing us to solve the NPL-PS problem by the local/global mesh deformation is based on the observation that the values of $\{\mathbf{n}_{i,j}\}$ determined by Eq.(6) are similar to the ground truth when the initial values of

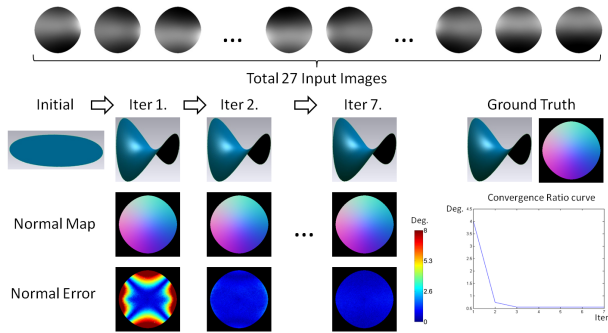


Figure 3. Experimental test on a saddle surface shows the progressive results of our framework. The top row gives 8 examples of total 27 input images under the illumination of different light sources. The ratio between the object’s dimension and the object-to-light distance in z -dimension is 0.37, which is under the illumination of NPL. Different columns show the progressive results obtained during the iteration. The errors on reconstructed normals are measured in terms of angle degree and displayed as color maps (see the bottom row).

$\{c_{i,j}\}$ are given in the working envelope of the acquisition system. After that, when using the updated $\{c_{i,j}\}$ obtained from the global blending to generate a new set of $\{n_{i,j}\}$, the shape is more similar to the real shape than the first update. Therefore, in our framework, these two steps are iteratively applied until the values of $\{c_{i,j}\}$ converge. The progressive results tested on a saddle surface is given in Fig.3, where the inputs includes 27 images illuminated by different near point lighting sources.

5. Experimental Results

We have implemented our approach in MATLAB and tested its performance on a variety of models. In the experimental tests, we reconstruct models from 2D images under the illumination of near point lighting. The results are compared with that are reconstructed from the same set of 2D images but under the conventional parallel lighting assumption. All the results are generated on an Intel i7 CPU with 3.4GHz and 8GB RAM in around 10 to 180 seconds at different resolutions. Results show that our new NPL-PS framework significantly outperforms the conventional ones.

First of all, we build a virtual environment for generating the images of NPL with the help of OpenGL library. For each model to be tested, 27 images under the NPL illumination are generated. According to the requirement of our NPL-PS framework, the images and the coordinates of 27 light sources are used as input to our program to generate 3D models. To compare with the conventional PS with parallel lighting, we use the vector from a model’s center to the positions of light sources as the parallel lighting directions to generate a dense normal field. After that, the *surface-from-gradients* (SfG) approach in [20] is employed to re-

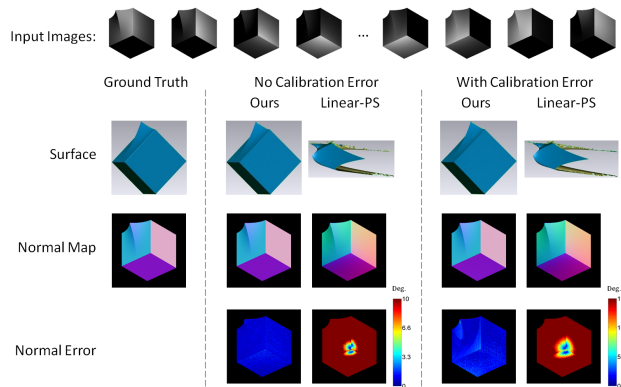


Figure 4. Experimental tests on a cubic model with sharp features under the illumination of NPL. The ratio between the object’s dimension and the object-to-light distance in z -dimension is 0.72. The top row shows eight example images of the total 27 input ones, the second row gives the reconstructed 3D surfaces, the third row provides the reconstructed normal maps, and the bottom row compares the reconstructed normal maps with the ground truth in the representation of color error maps. To verify the robustness of our approach, 5% random errors w.r.t. the working envelope’s width has been added to simulate the calibration errors.

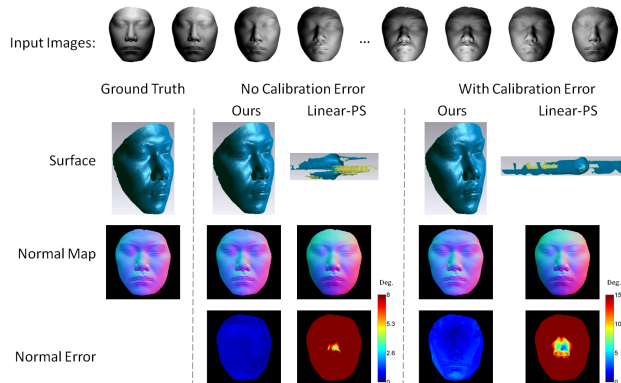


Figure 5. Experimental tests on a face model under the illumination of 27 near point light sources. The ratio between the object’s dimension and the object-to-light distance in z -dimension is 0.22.

construct the surface from a normal field. As the ground truth is known, we can evaluate errors on both the 3D shape and the normal map obtain from the conventional PS and ours. One example is shown in Fig.4. It is easy to find that the reconstruction from conventional PS is largely distorted as the object is put at a place very close to the light sources. To further verify the robustness of our approach, we randomly add errors at the level in 5% of the working envelope’s width onto the positions of light sources. This is to simulate the calibration errors that could be embedded. It can be found that our NPL-PS framework can also generate very accurate results under this noisy condition. Two more examples are also tested and shown in Figs.5 and 6. Errors on the positions of light sources are assigned in the

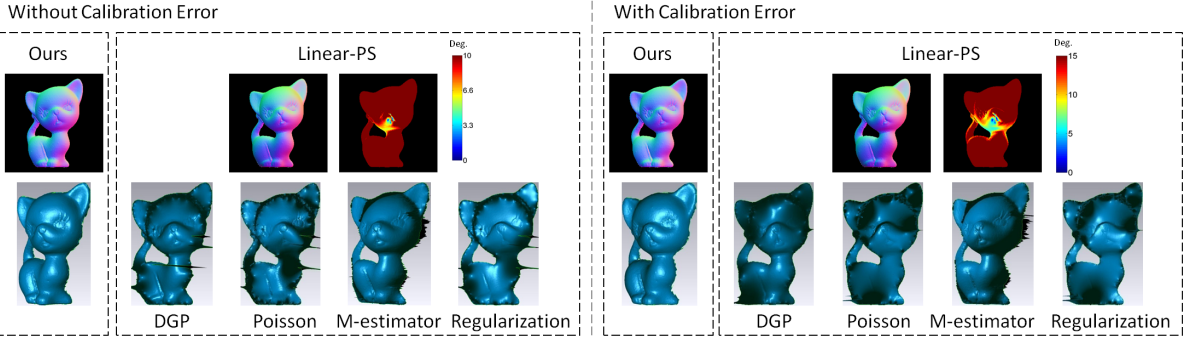


Figure 7. When parallel lighting is employed to generate normal maps for NPL, the shape error in low frequency band caused by the parallel lighting assumption cannot be resolved during the SfG reconstruction step. The results from DGP [20], Poisson [21], M-estimator [22] and regularization [23] are shown – all have large distortion in shape when linear-PS is used.

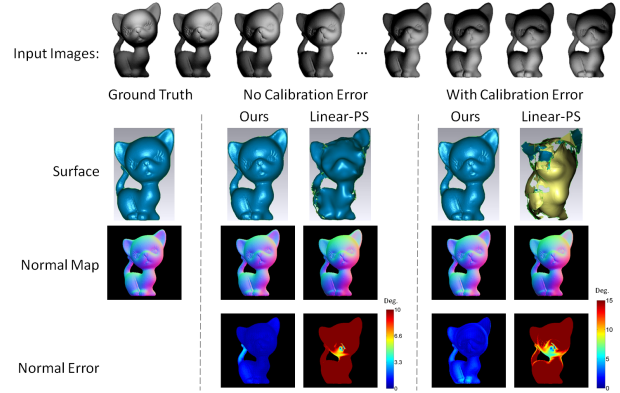


Figure 6. Experimental tests on a kitten model under the illumination of NPL. The resultant surface is reconstructed from 27 input image. The ratio between the object’s dimension and the object-to-light distance in z -dimension is 0.30.

same way as the cube example. The same conclusion can be made on these two examples – our NPL-PS framework can greatly improve the quality of reconstruction comparing to the conventional PS under the parallel lighting assumption. In all these examples, SfG reconstruction in the conventional PS is computed by [20]. To further verify that the shape errors are not generated by SfG, we test three more SfG techniques in Fig.7, which include Poisson [21], M-estimator [22] and regularization [23].

Another test is taken to verify the performance of our approach when the object to be reconstructed is placed at different distances from the light sources. The average errors on the normals estimated by our NPL-PS and the parallel lighting PS are measured. The testing results on the cube example are shown in Fig.8. It is found that when the model is placed far away from the light sources, both the parallel PS and our NPL-PS approaches can generate accurate results with small distortion. The reconstruction based on parallel PS becomes worse and worse when increasing the ratio between the object diameter and the object-to-light

Table 1. Statistics on Computing Time[†]

Model	Figure	Time on Different Resolutions		
		128 ²	256 ²	512 ²
Cubic	4	21.2 sec.	50.5 sec.	131 sec.
Face	5	10.1 sec.	32.6 sec.	102 sec.
Kitten	6	28.3 sec.	60.1 sec.	180 sec.

[†]The total time of computation converging within 10 iterations is reported, where the time of pre-factorization has been included.

distance (i.e., reducing the object-to-light distance). However, the NPL-PS method proposed in this paper is nearly not affected. The same phenomenon is observed when the positions of light sources have been embedded with calibration errors (see the right of Fig.8).

The local/global deformation based computation can solve the nonlinear NPL-PS problem in a very efficient way. Statistics of applying our approach on input images with rectangular domain in different resolutions are listed in Table 1. The statistics are generated on our primary implementation in MATLAB. We plan to implement our approach by C++ to further improve the efficiency of computation in the near future.

To further verify the performance of our approach in real environment, we have constructed a hardware setup for near point lighting PS. As shown in Fig.9, ten light bubbles are installed around a camera. The 3D object to be reconstructed is placed on the white board to be illuminated by these 10 near point lighting sources. We calibrate the light sources positions in the following way. Two shiny hemispheres are employed to calibrate the position of each light source. Motivated by [13], the lighting direction of a light source according to the center of a shiny hemi-sphere can be obtained. After such two such lines are calibrated, the middle of the minimal distance segment between them are estimated as the final position of a light source. The 3D terrain surface from a piece of crumpled paper has been

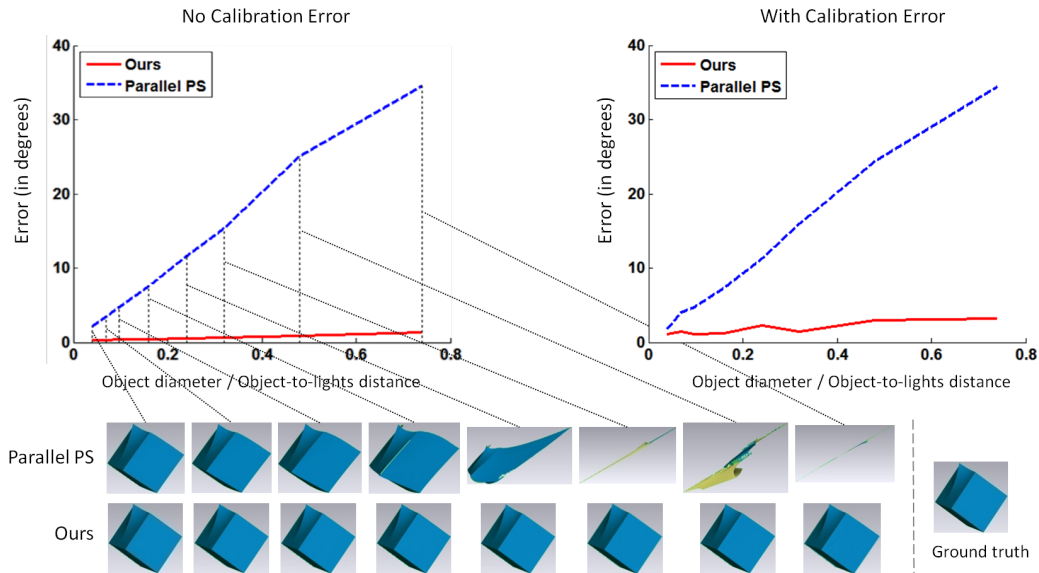


Figure 8. Comparison in the virtual environment by using 1) images taken in the exposure of far point lighting in the parallel PS to 2) images taken in the NPL exposure in our framework. To obtain nearly parallel lighting in case 1), the light sources must be placed far ways from the object to be reconstructed. As a result, the captured images become too dark to be used in reconstruction the shape. This comparison is actually as using the left point on the blue curve to compare with other points on the red curve. Here it assumes a very strong light source. In practice, when a light-source with lower intensity is employed, larger errors will be generated on the reconstruction from parallel PS.

captured by this setup and shown in Fig.10. From the input 10 images, a piecewise linear 3D surface of the paper can be successfully reconstructed. It can be found from the hardware setup that the illumination is taken under the near point lighting condition. The ratio between the object's dimension and the object-to-light distance in z -axis is around 0.45 in this example. The surface reconstructed on this hardware NPL-PS setup looks real and very similar to the true surface of the crumpled paper. As lack of ground truth, the test is taken on a flat plane. The error is quantitatively measured by the height difference obtained from the reconstructed mesh 0.216mm is observed in a sensing region with 55mm x 35mm. Moreover, we test the reconstruction on a saw-teeth shape with teeth height 12.22mm. Our reconstruction shows a result with teeth height 9.73mm. The error is mainly caused by the unstable lighting intensity and the assumption of Lambertian lighting model which is not exactly true in practice. To further measure the accuracy of our results, ground truth of the tested surface must be known. In our future work, we plan to first use 3D printing to fabricate a surface according to a mesh model [25]. After that, the fabricated model is placed on our setup to test. The reconstructed 3D surface will be compared with the original mesh model to verify the accuracy and the performance of our system.

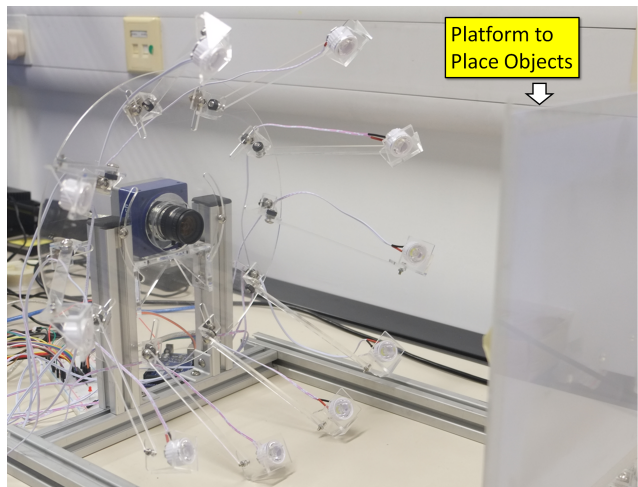


Figure 9. A hardware setup for photometric stereo with near point lighting – 10 NPL sources are placed around a camera with very close distance to the objects placed on the white board.

6. Conclusion

In this paper, we present a novel computational framework to deal with the bottleneck of near point lighting model in the photometric stereo. We formulate such a nonlinear PS problem in a pure geometry way and solve it through the local/global mesh deformation. The surface normals and depths can be simultaneously estimated in our

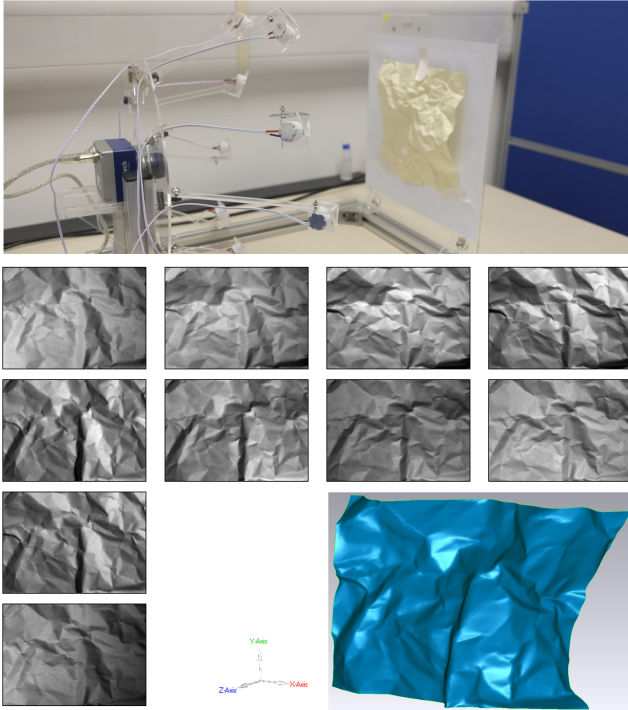


Figure 10. Using our hardware setup for NPL-PS, the 3D terrain surface of a crumpled paper can be successfully reconstructed.

approach. The effectiveness of our method has been demonstrated using synthetic images with calibration errors considered. A hardware setup for NPL-PS has been constructed to further verify the performance of our technique presented in this paper. The distinct advantage of this new technique is its ability to efficiently generate dense 3D depth maps in high accuracy. To the best of our knowledge, this has not been realized by any prior method.

References

- [1] S. Barsky and M. Petrou. The 4-source photometric stereo technique for three-dimensional surfaces in the presence of highlights and shadows. *IEEE Transactions on Pattern Analysis and Machine Intelligence*, 25(10):1239–1252, 2003.
- [2] D. Nehab, S. Rusinkiewicz, J. Davis, and R. Ramamoorthi. Efficiently combining positions and normals for precise 3d geometry. *ACM Trans. Graph.*, 24(3):536–543, 2005.
- [3] A. Hertzmann and S.M. Seitz. Example-based photometric stereo: Shape reconstruction with general, varying brdfs. *IEEE Transactions on Pattern Analysis and Machine Intelligence*, 27(8):1254–1264, 2005.
- [4] D.B. Goldman, B. Curless, A. Hertzmann, and S.M. Seitz. Shape and spatially-varying brdfs from photometric stereo. *IEEE Transactions on Pattern Analysis and Machine Intelligence*, 32(6):1060–1071, 2010.
- [5] R.J. Woodham. Photometric method for determining surface orientation from multiple images. *Optical engineering*, 19(1):139–144, 1980.
- [6] L. Wu, A. Ganesh, B. Shi, Y. Matsushita, Y. Wang, and Y. Ma. Robust photometric stereo via low-rank matrix completion and recovery. In *Proceedings of 2011 ACCV Conference*, pages 703–717, 2011.
- [7] A.S. Georghiadis. Incorporating the torrance and sparrow model of reflectance in uncalibrated photometric stereo. In *Proceedings of Ninth IEEE International Conference on Computer Vision*, pages 816–823, Oct 2003.
- [8] N. Alldrin, T. Zickler, and D. Kriegman. Photometric stereo with non-parametric and spatially-varying reflectance. In *IEEE Conference on Computer Vision and Pattern Recognition*, pages 1–8, 2008.
- [9] W. Xie, Z. Song, and X. Zhang. A novel photometric method for real-time 3d reconstruction of fingerprint. In *Proceedings of the 6th International Conference on Advances in Visual Computing - Volume Part II*, pages 31–40, 2010.
- [10] F. Lu, Y. Matsushita, I. Sato, T. Okabe, and Y. Sato. Uncalibrated photometric stereo for unknown isotropic reflectances. In *Proceedings of the 2013 IEEE Conference on Computer Vision and Pattern Recognition*, pages 1490–1497, 2013.
- [11] H.-S. Chung and J. Jia. Efficient photometric stereo on glossy surfaces with wide specular lobes. In *IEEE Conference on Computer Vision and Pattern Recognition*, 2008.
- [12] T. Higo, Y. Matsushita, and K. Ikeuchi. Consensus photometric stereo. In *IEEE Conference on Computer Vision and Pattern Recognition*, 2010.
- [13] T. Higo, Y. Matsushita, N. Joshi, and K. Ikeuchi. A handheld photometric stereo camera for 3-d modeling. In *IEEE International Conference on Computer Vision*, pages 1234–1241, 2009.
- [14] Z. Zhou and P. Tan. Ring-light photometric stereo. In *Proceedings of the 11th European Conference on Computer Vision: Part II, ECCV'10*, pages 265–279, 2010.
- [15] Thoma Papadhimetri and Paolo Favaro. Uncalibrated near-light photometric stereo. In *Proceedings of the British Machine Vision Conference*. BMVA Press, 2014.
- [16] A. Wetzler, R. Kimmel, A.M. Bruckstein, and R. Mecca. Close-range photometric stereo with point light sources. In *3D Vision (3DV), 2014 2nd International Conference on*, volume 1, pages 115–122, Dec 2014.
- [17] Fumihiko Sakaue and Jun Sato. A new approach of photometric stereo from linear image representation under close lighting. In *Computer Vision Workshops (ICCV Workshops), 2011 IEEE International Conference on*, pages 759–766. IEEE, 2011.
- [18] O. Sorkine and M. Alexa. As-rigid-as-possible surface modeling. In *Proceedings of the Fifth Eurographics Symposium on Geometry Processing*, pages 109–116, 2007.
- [19] S. Bouaziz, M. Deuss, Y. Schwartzburg, T. Weise, and M. Pauly. Shape-up: Shaping discrete geometry with projections. *Computer Graphics Forum*, 31(5):1657–1667, 2012.

- [20] W. Xie, Y. Zhang, C.C.L. Wang, and R.C.-K. Chung. Surface-from-Gradients: An approach based on discrete geometry processing. In *IEEE Conference on Computer Vision and Pattern Recognition (CVPR)*, pages 2203–2210, 2014.
- [21] T. Simchony, R. Chellappa, and M. Shao. Direct analytical methods for solving poisson equations in computer vision problems. *IEEE Transactions on Pattern Analysis and Machine Intelligence*, 12(5):435–446, 1990.
- [22] P. Charbonnier, L. Blanc-Feraud, G. Aubert, and M. Barlaud. Deterministic edge-preserving regularization in computed imaging. *IEEE Transactions on Image Processing*, 6(2):298–311, 1997.
- [23] G. Aubert and P. Kornprobst. *Mathematical Problems in Image Processing: Partial Differential Equations and the Calculus of Variations (Applied Mathematical Sciences)*. Springer-Verlag New York, Inc., 2006.
- [24] W. Zhou and C. Kambhamettu. Estimation of illuminant direction and intensity of multiple light sources. In *Proceedings of the 7th European Conference on Computer Vision-Part IV, ECCV '02*, pages 206–220, 2002.
- [25] C.C.L. Wang and T. Chen. Thickening freeform surfaces for solid fabrication. *Rapid Prototyping Journal*, 19(6):395–406, 2013.